J Mater Sci (2013) 48:1940–1946
DOI 10.1007/s10853-012-6959-0

Spark plasma sintering and thermoelectric evaluation of nanocrystalline magnesium silicide (Mg_2Si)

M. Saleemi · M. S. Toprak · S. Fiameni · S. Boldrini · S. Battiston · A. Famengo · M. Stingaciu · M. Johnsson · M. Muhammed

Received: 6 July 2012 / Accepted: 12 October 2012 / Published online: 23 October 2012
© Springer Science+Business Media New York 2012

Abstract Recently magnesium silicide (Mg_2Si) has received great interest from thermoelectric (TE) society because of its non-toxicity, environmental friendliness, comparatively high abundance, and low production material cost as compared to other TE systems. It also exhibited promising transport properties, including high electrical conductivity and low thermal conductivity, which improved the overall TE performance (ZT). In this work, Mg_2Si powder was obtained through high energy ball milling under inert atmosphere, starting from commercial magnesium silicide pieces (99.99 %, Alfa Aesar). To maintain fine microstructure of the powder, spark plasma sintering (SPS) process has been used for consolidation. The Mg_2Si powder was filled in a graphite die to perform SPS and the influence of process parameters as temperature, heating rate, holding time and applied pressure on the microstructure, and densification of compacts were studied in detail. The aim of this study is to optimize SPS consolidation parameters for Mg_2Si powder to achieve high density of compacts while maintaining the nanostructure. X-Ray diffraction (XRD) was utilized to investigate the crystalline phase of compacted samples and scanning and transmission electron microscopy (SEM & TEM) coupled with Energy-Dispersive X-ray Analysis (EDX) was used to evaluate the detailed microstructural and chemical composition, respectively. All sintered samples showed compaction density up to 98 %. Temperature dependent TE characteristics of SPS compacted Mg_2Si as thermal conductivity, electrical resistivity, and Seebeck coefficient were measured over the temperature range of RT 600 °C for samples processed at 750 °C, reaching a final ZT of 0.14 at 600 °C.

M. Saleemi (✉) · M. S. Toprak (✉) · M. Muhammed
Functional Materials Division, KTH Royal Institute of Technology, Kista, Stockholm, Sweden
e-mail: mohsins@kth.se

M. S. Toprak
e-mail: toprak@kth.se

S. Fiameni · S. Boldrini · S. Battiston · A. Famengo
CNR, Institute for Energetics and Interphases (IENI-CNR), Corso Stati Uniti 4, I-35127 Padua, Italy

M. Stingaciu · M. Johnsson
Department of Materials and Environmental Chemistry, Stockholm University, Stockholm, Sweden

Introduction

Thermoelectric (TE) devices are promising candidates for recycling of waste heat and a potential substitute for power generation. TE devices have many advantages as direct inter-conversion between electrical and thermal energy, being solid state devices with no moving parts, silent, portable, etc., [1]. TE materials' efficiency is represented by the figure of merit; $ZT = S^2T/\rho\kappa$ where S represents the Seebeck coefficient, T is the absolute temperature, ρ is the electrical resistivity, and κ is the thermal conductivity [1, 2]. There are many reports where TE materials with high power factor (S^2/ρ) and low κ, showed increased overall performance [3, 4]. Recently, TE research have progressed remarkably by the development of nanostructured materials, such as 0D-quantum dots [5], 1D-nanowires and nanotubes [6], 2D-superlattices [7, 8], and 3D-bulk nanostructures [9, 10]. Furthermore, bulk nanostructured (BN) samples fabricated by novel chemical [11] or physical routes showed a high ZT value compared with conventional production routes [12]. The compounds of Mg_2G^{IV} (G^{IV} = Si, Ge and Sn) and its alloys have been recognized

as interesting candidates for the study of TE applications by Nikini et al. [13], and these compounds demonstrated improved ZT performance in intermediate temperature range (400–800 K) [14, 15]. They are identified as non-toxic, abundant in nature and less expensive materials as compared to the state of the art conventional TE materials like clathrates, chalcogenides, and skutterudites [16].

Magnesium Silicide (Mg_2Si) is a narrow band gap semiconductor (Eg $\sim$ 0.3–0.6 eV), with low density (below 2 g/cm^3) and high melting temperature ($\sim$1000 °C) [17]. Mg_2Si and its alloys consist of anti-fluorite crystal structure with Si in FCC (face centered cubic) sites and Mg in tetrahedral positions [18]. It was claimed by simulation in Zaitsev et al. [19], that this type of TE materials can attain greater ZT values because of high charge mobilities, containing large effective masses and comparatively low lattice component of thermal conductivity. For the past decades, this class of materials has been under investigation for mid-to-high temperature range of TE applications. Ball-milling technique is a well-known method for brittle material production; but the ductile characteristics and reactivity of Mg with oxygen make this synthesis process a nontrivial route. [20].

There are, however, few reports on the synthesis parameters and improved ball-milling methods to manufacture nanocrytalline Mg_2Si powder [20–22]. However optimization of sintering parameters is required to obtain ideal densification and microstructure. In this work, nanocrystalline Mg_2Si materials were prepared by ball-milling process and spark plasma sintering (SPS) process was used for consolidation. In particular, SPS consolidation parameters were investigated to achieve the highest compaction density and conserve the nanostructured grains in the sintered pellets, by studying different temperature and holding time for SPS experiments. Crystallite size and crystalline phase identification were performed by XRD, SEM, and TEM techniques; detailed microstructure analyses from the fractured surfaces of compacts are presented.

Experimental methods

Powder processing

Magnesium Silicide (Mg_2Si) powders were manufactured from commercially available high purity magnesium silicide pieces (99.99 %, Alfa Aesar). The raw materials were ground under Argon (Ar) atmosphere in a planetary ball mill (BM) with hexane as dispersion medium. BM process was accomplished in 24 h with an optimized rotational speed of 330 rpm. Afterward, the consolidation of Mg_2Si powder was achieved under Ar atmosphere using Dr Sinter 2050 Spark plasma sintering (SPS—imported from Sumitomo Coal Mining Co., Tokyo, Japan) using a graphite die with 15 mm inner diameter. A minimal amount of 2 g of Mg_2Si was loaded into the die for the sintering experiments. Important SPS parameters such as the sintering temperature and holding time were studied to achieve the best compaction conditions for Mg_2Si pellets. All the samples were prepared at a constant heating rate of 100 °C/min, and constant applied pressure 8.8 kN. Two different sintering temperatures at 750 and 850 °C were used and three various holding times as 0, 2, and 5 min were applied to investigate their effect on density and grain size of compacts.

Characterizations

The crystalline phases were identified by X-ray diffraction (XRD) using a Philips X'pert pro super diffractometer with a Cu Kα source ($\lambda = 1.5418$ Å) at operating voltage 40 kV and applied current 40 mA. The Rietveld refinement of the XRD profiles has been exploited to obtain information about phase amounts, crystallite sizes, and lattice parameters [23]. Scanning electron microscopy (SEM) and Energy-dispersive X-ray analysis (EDX—at a standard working distance of 8 mm and an accelerating voltage of 20 kV) were performed using Zeiss Ultra 55 SEM system. Transmission electron microscopy (TEM) was performed using a JEOL 2100F TEM, and selected area electron diffraction (SAED) was also performed to investigate structural homogeneity at particulate level. TEM samples were prepared by dispersing a finite amount of Mg_2Si powder in ethanol and finally dropping the solution onto a carbon coated grid. The thermal diffusivity and the specific heat of the samples were measured by a laser flash apparatus (Netzsch LFA 457 MicroFlash®). The thermal conductivity κ was calculated according to the formula $\kappa = \alpha \rho C_p$ where α is the thermal diffusivity, ρ is the density, and C_p is the specific heat of the material. The Seebeck coefficient (S) and the electrical resistivity (ρ) were measured from RT up to 600 °C using a custom test apparatus described elsewhere. All measurements were carried out under Ar atmosphere. Finally, the dimensionless figure of merit was calculated using the equation; $ZT = S^2T/\rho\kappa$.

Results and discussion

Synthesized nanocrystalline Mg_2Si powder was sintered by SPS technique, and the optimized compaction parameters were identified via a series of experiments. The most significant SPS parameters are sintering temperature, applied pressure, heating rate and holding time. Sample IDs and the SPS parameters utilized for the experiments are presented in Table 1. The results shown in Table 1 can be used to explain the effect of these critical parameters on the compaction density and the crystallite size. Three different sintering temperatures at 650, 750, and 850 °C were

selected for 5 min holding time for the first set of experiments. The sample compacted at 650 °C has achieved a densification of only 85 %. The samples compacted at 750 and 850 °C were further compacted for 2 and 0 min holding time at respective temperatures.

Powder XRD analysis was performed to determine the crystal phases: Fig. 1a–i presents several XRD patterns from the as prepared and compacted Mg_2Si nanopowder and compacts obtained under different SPS parameters (as detailed in Table 1). XRD pattern from pristine bulk Mg_2Si is shown in Fig. 1a and it confirms some contamination of oxides and Si impurities. Figure 1b clearly shows after ball milling Mg_2Si has major crystalline phase, and it also revealed that traces of MgO and Si phases are still present in the ball-milled Mg_2Si powder. The presence of MgO and Si originate from raw starting materials and partly due to the oxidation of Mg_2Si during the BM process [24]. XRD patterns from Mg_2Si powder and compacted samples were indexed using reference patterns for Mg_2Si (JCPDS# 00-035-0773), MgO (JCPDS# 00-045-0946), and Si (JCPDS# 04-001-7247). Figure 1c–i clearly show that the peak intensity of free Si is reducing during the SPS processing. It is also important to note that the XRD peaks of BM Mg_2Si powder are significantly broader as compared to the sintered samples revealing the increase in crystallite size of the compacted samples under sintering conditions.

The presence of MgO phase is detrimental for TE performance of silicide, as reported by Fiameni et al. [25]. The pristine materials contain about 6 % of the MgO phase as reported in earlier works [25]. All the samples sintered at 750 °C present lower MgO amounts (10 %) with respect to the samples sintered at 850 °C (in as much as approximately 19 %). Rietveld refinement was employed to estimate the crystallite size and the average crystallite size is reported in the range from 120 to 240 nm (See Table 1). The geometrical (d = m/V) and theoretical density values (Rietveld refinement) are reported in Table 1 for samples sintered at 650, 750, and 850 °C at different holding times. All the samples indicate a density higher than 91 % with the exception of the samples sintered at 650 °C showing a density lower than 80 %. For this reason, compacts at 650 °C were not considered for the TE evaluation. XRD results show that the crystallite size grew severely during the consolidation, particularly for the sample sintered at 850 °C for different holding time. Moreover, it also shows more densification but compensated with a larger crystallite size. Due to the high compaction density and lower crystallite size, pellets compacted at 750 °C, were considered for further TE evaluations.

SEM micrographs obtained from the fabricated and SPS compacted samples are shown in Fig. 2a–h. Micrograph of as synthesized nanocrystalline Mg_2Si, presented in Fig. 2a, reveals irregular particle morphology and the presence of

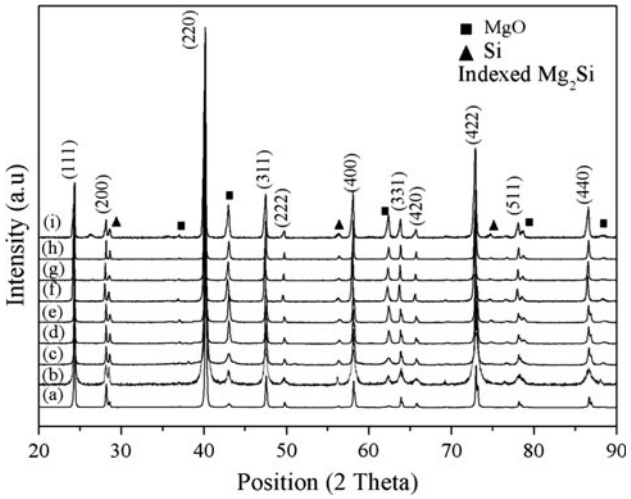

Fig. 1 Powder X-Ray Diffraction Patterns; *a* Pristine bulk Mg_2Si; *b* Synthesized nanocrystalline Mg_2Si Powder, SPS sample; *c* *MS_01, *d* MS_02, *e* MS_03, *f* MS_04, *g* MS_05, *h* MS_06, and *i* MS_07

Table 1 SPS parameters, compaction densities, and average crystallite size of Mg_2Si samples

Sample id	SPS parameters			Geometrical density (g/cm^3)	Theoretical density (g/cm^3)	Compaction density (%)	Average crystallite size (nm)
	Temperature (°C)	Pressure (kN)	Holding time (min)				
MS_As-prepared	NA	NA	NA	NA	2.06	NA	50
MS_01[a]	650	8.8	5	2.49	2.13	85.4	120
MS_02	750	8.8	5	2.38	2.19	91.5	150
MS_03	850	8.8	5	2.32	2.23	95.8	120
MS_04	750	8.8	2	2.28	2.19	96.2	150
MS_05	850	8.8	2	2.25	2.19	97.1	200
MS_06	750	8.8	0	2.19	2.13	97.2	240
MS_07	850	8.8	0	2.29	2.21	96.2	180

[a] Could not achieve the acquired densification, therefore it was not considered for TE evaluation

few small aggregates. In order to estimate the average grain size, Image J software was used to measure the individual particles ($n > 300$). Most of the particles measured were in the range of 100–400 nm while the average particle size is estimated as 230 ± 30 nm. The wide distribution in the primary particle size is due to different impact of ball-milling process. Detailed chemical composition analysis, performed by coupled EDX, results showed the presence of excessive Mg, O, and Si elements; which supports the XRD results in that the MgO and free Si phases are present in the ball-milled Mg_2Si powder.

Figure 2b–h show the detailed microstructural analyses from the fractured surfaces of SPS samples compacted under various conditions. Figure 2b shows the internal structures of the grains when BM Mg_2Si was compacted at 650 °C at a holding time of 5 min. The density calculation shows (See, Table 1) a low compaction density and the fractured surface microstructure contains portions of pores/voids (Fig. 2b). In Fig. 2c, d micrographs from the SPS samples at 750 and 850 °C with 5 min holding time are presented, which show less porosity and more evenly distributed grain growth. The compaction density results,

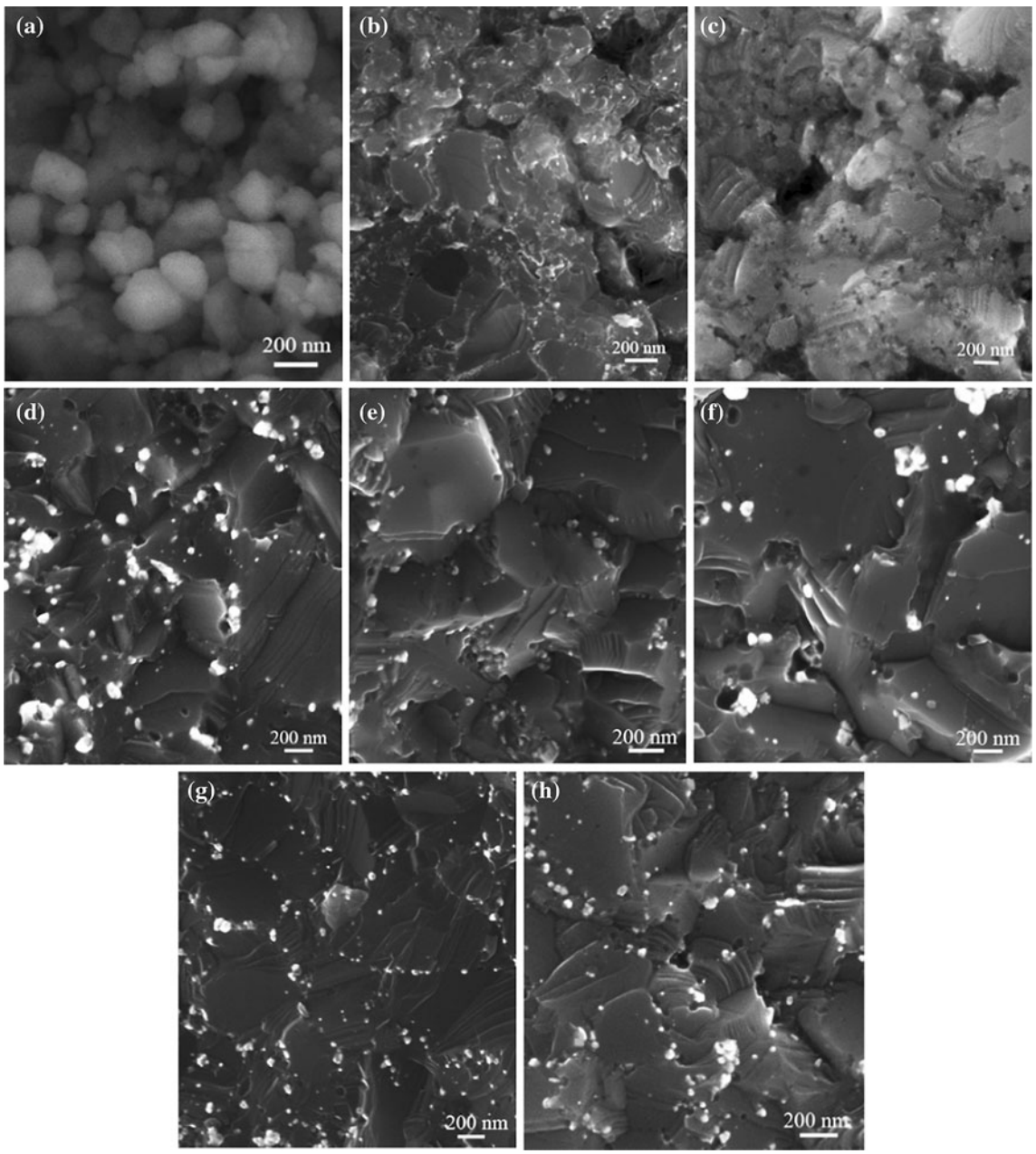

Fig. 2 SEM micrographs of; **a** As synthesized nanocrystalline Mg_2Si powder; the fractured surfaces of SPS compacted Mg_2Si at; **b** 650 °C for 5 min, **c** 750 °C for 5 min, **d** 850 °C for 5 min, **e** 750 °C for 2 min, **f** 850 °C for 2 min, **g** 750 °C for 0 min, and **h** 850 °C for 0 min

from the samples compacted at 750 and 850 °C, were selected for further investigation of sintering with different holding times. Figure 2e–h show the fractured surfaces of SPS sintered samples at 750 and 850 °C for 2 and 0 min holding times, respectively. It was observed that short holding time (like 0 min) causes less grain growth and the grain size did not increase more than 400 nm. On the other hand, increasing the holding time increases the compaction density, but it compensates with an extensive grain growth with grain size reaching to 1 μm at holding time 2 and 5 min. Longer holding time may affect the grain growth/coarsening, ending up with non-optimal TE properties. Hence, an optimum grain size with sufficient compaction density is expected to lead to the best combination of transport properties.

TEM analysis was carried out to evaluate the microstructure and the presence of different phases using the electron diffraction (ED) and dark field (DF) microscopy; few micrographs are presented in Fig. 3a–d. TEM image in Fig. 3a presents BM Mg_2Si, where particles with an average size of 200 nm are observed-in agreement with the SEM grain size estimation. Different contrast in this image may results from the defect produced in the material during ball milling or it may also reflect the presence of secondary phases (MgO or Si). ED pattern from the BM Mg_2Si, Fig. 3b, is taken from the grain shown in Fig. 3c. ED pattern characteristics show that the material is polycrystalline, as well as the presence of Mg_2Si as the major and MgO as minor phases in the material. The phases observed in ED pattern were indexed using the same set of PDF reference patterns (Pdf# 035-0773 (*for Mg_2Si*), and Pdf# 045-0946 (*for MgO*)) utilized for XRD phase identification. Furthermore, Figure 3c, d shows the bright field and dark field TEM images, which clearly elucidate the differences in the contrast. Particularly, in the dark field image one can observe two different phases with white (MgO) and black (Mg_2Si) contrast. EDX analysis was also performed on this site to confirm the elemental composition. Based on XRD and TEM (ED) characterizations, it is observed that highly reactive Mg can diffuse out of the Mg_2Si crystal, forming impurity phases of MgO and Si. This requires further strict control of reaction environment to avoid any possible contact with oxygen for the preparation of high purity Mg_2Si powder.

XRD and SEM analyses show that the optimal temperature for SPS sintering of BM Mg_2Si is 750 °C. Since the source material has the same history, samples are evaluated further to understand the influence of observed compaction density and grain size characteristics. For this reason, TE characterizations were performed on the samples sintered

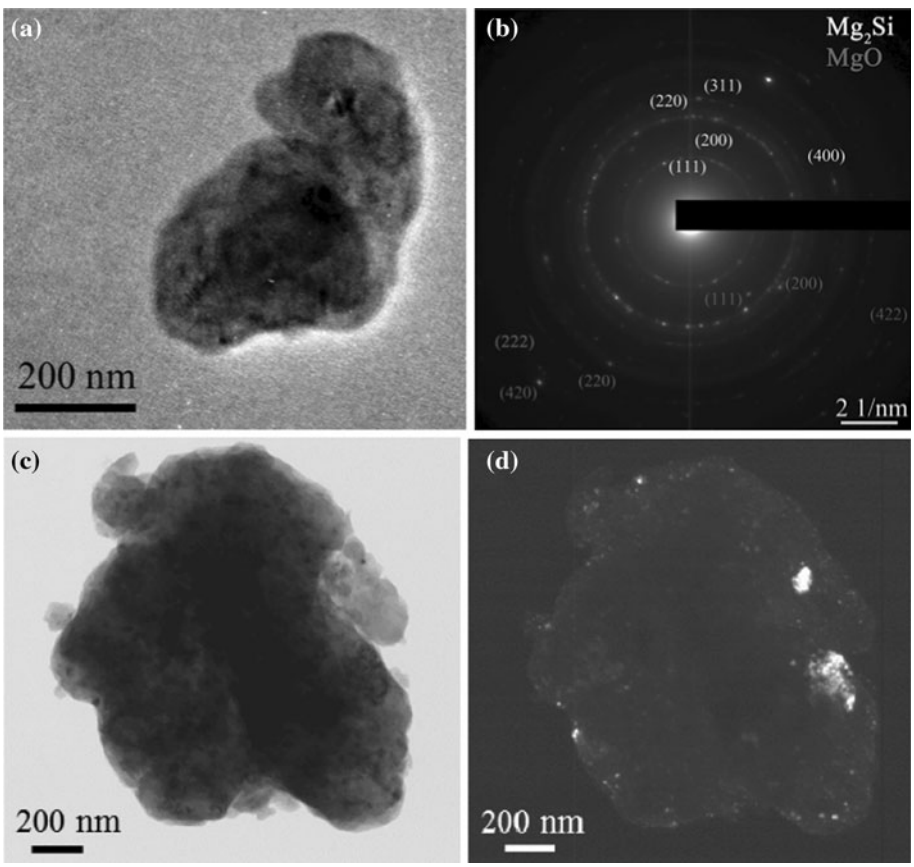

Fig. 3 **a** TEM micrograph of as prepared Mg_2Si, **b** ED pattern, **c** Bright, and **d** Dark field TEM images

at 750 °C with different holding times (5, 2 and 0 min). Figure 4a–d show the detailed TE characterizations performed from room temperature up to 600 °C. All the samples sintered at 750 °C (MS_02, 04 and 06) exhibit a negative Seebeck coefficient Fig. 4a, indicating n-type conduction. Its absolute value increased up to 250 °C, reaching a value of −475 μV/K, than started the decrease reaching −200 μV/K at 600 °C. Electrical resistivity, presented in Fig. 4b, of the sample compacted at 750 °C for 2 min holding time, showed almost two to three times lower resistivity at room temperature as compared to the samples prepared at 5 and 0 min holding times. Decreasing electrical resistivity with an elevation in temperature may reflect non-degenerate semiconductor characteristics. Our results of Seebeck coefficient and electrical resistivity are in agreement with the earlier reports on undoped Mg_2Si [26, 27]. Thermal conductivity results are presented in Fig. 4c which shows RT κ of 10–12 W/mK which decreases with increase in temperature. Thermal conductivity values of synthesized nanocrystalline Mg_2Si sample (Fig. 4c) are comparable to that reported by Martin J. J. [28], in which multigrain Mg_2Si crystal was synthesized using Bridgman method. Synthesized material show conventional extrinsic semiconductor behavior as with the increase of temperature thermal conductivity values decrease, as reported for multigrain Mg_2Si crystals. [28]. In some reports, further reduction in κ is considered as a tedious challenge to improve the TE properties of Mg_2Si based compounds [29]. Bux et al. proved that the reduction in κ is mainly attributed to phonon scattering at the grain boundaries and nanostructuring can increase this phenomenon, by increasing the density of grain boundaries, to attain the goal [28]. During materials synthesis and processing step, the formation of bigger grains may lead to deprived phonon interaction and thus poor TE properties, similar reasons reported in different TE material systems [30]. Figure 4d shows the calculated dimensionless figure of merit (ZT); the sample compacted at 750 °C for 2 min holding time at 8.8 kN pressure achieved a ZT value of 0.14, which is slightly higher value compared to that of previously reported undoped Mg_2Si [24, 31]. It can be observed that samples compacted at 750 °C for 5 and 0 min holding time did not show different behavior because of the large grain growth; the ZT value from these two samples were quite similar as earlier observed and reported by Cederkrantz et al. [30].

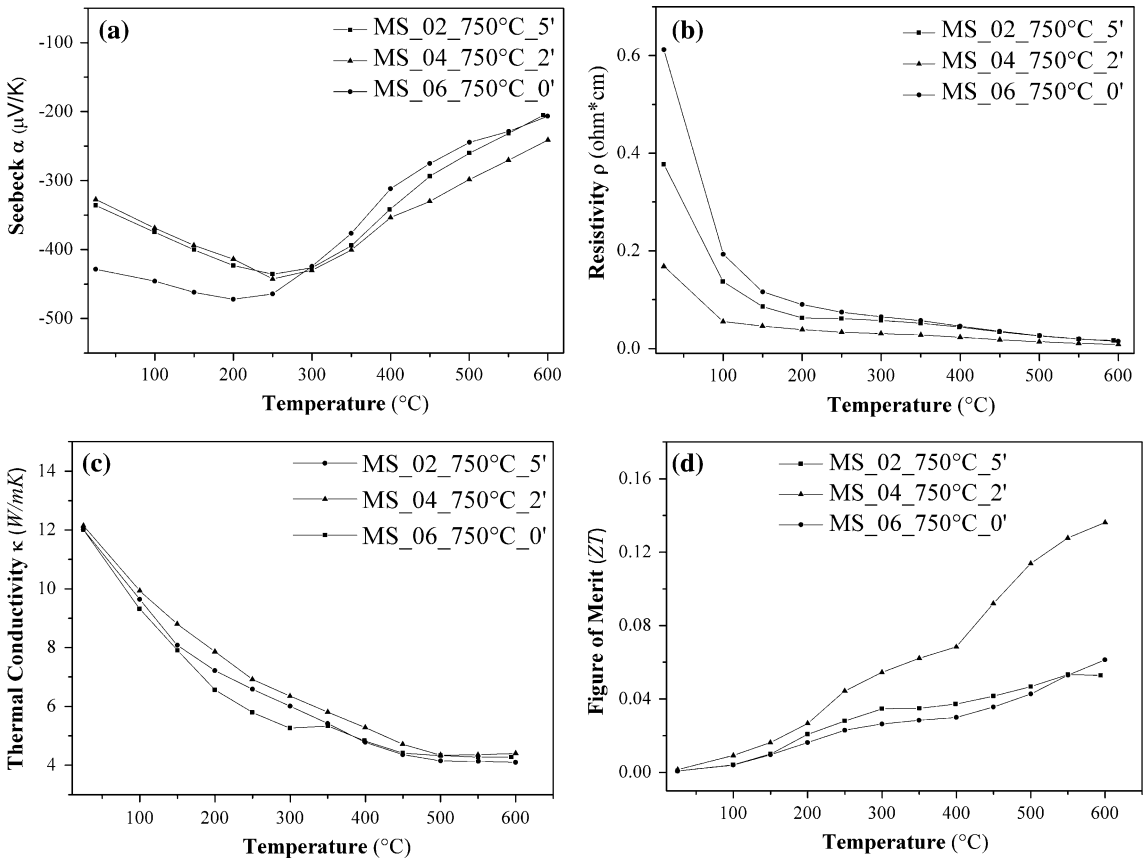

Fig. 4 Temperature dependence of **a** seebeck, **b** resistivity, **c** thermal conductivity, and **d** calculated figure of merit (ZT) of SPS compacted samples at 750 °C with holding times of 5, 2 and 0 min

Conclusions

The n-type Mg_2Si nanopowder was prepared by wet ball-milling method and successfully used to fabricate highly dense pellets using SPS. Detailed physicochemical characterization results revealed that the as prepared powder exhibited a crystallite size of 230 nm, reflecting the success of nanostructuring attempts. Phase analysis revealed the presence of secondary phases of MgO and Si, which originate from the raw material. Critical SPS process parameters as sintering temperature and holding time were investigated to optimize the consolidation parameters for the compaction of undoped Mg_2Si. We optimized the parameters to maintain the nanostructure and achieve a high compaction density during the SPS process. Based on the compaction density and grain size evaluation, samples processed at 750 °C were chosen for further TE property evaluation. A ZT value $\sim$0.14 at 600 °C was obtained for SPS compacted sample at 750 °C for 2 min holding time—with grain size of in the range of 300–400 nm and 97 % compaction density. It is suggested through further optimization of Mg_2Si nanopowder synthesis with high purity (the absence of oxide phases) and through doping, it is possible that one can achieve a promising Mg_2Si-based TE material for power generation applications.

Acknowledgements This work has been funded by Swedish Foundation for Strategic Research–SSF (grant no: EM11-0002) and the Italian National Research Council–Italian Ministry of Economic Development Agreement "Ricerca di sistema elettrico nazionale." The authors would like to thanks to Hans Bergqvist for TEM measurements.

References

1. Dresselhaus MS, Chen G, Tang MY, Yang R, Lee H, Wang D, Ren Z, Fleurial J-P, Gogna P (2007) Adv Mater 19:1043
2. Rowe DM (1995) CRC handbook of thermoelectrics. CRC Press LLC, Boca Raton
3. Snyder GJ, Toberer ES (2008) Nature Mater 7:105
4. Hicks LD, Harman TC, Sun X, Dresselhaus MS (1996) Phys Rev B 53:R10493
5. Toprak M, Muhammed M (2006) CRC Thermoelectrics Handbook. CRC Press LLC, Boca Raton
6. Harman T, Walsh M, Laforge B, Turner G (2005) J Electron Mater 34:L19
7. Harman TC, Taylor PJ, Walsh MP, LaForge BE (2002) Science 297:2229
8. Li S, He Z, Toprak M, Stiewe C, Mueller E, Muhammed M (2007) Phys Status Solidi RRL 6:259
9. He ZM, Stiewe C, Platzek D, Karpinski G, Muller E, Li SH, Toprak M, Muhammed M (2007) J Appl Phys 101:043707
10. Poudel B, Hao Q, Ma Y, Lan YC, Minnich A, Yu B, Yan X, Wang DZ, Muto A, Vashaee D, Chen XY, Liu JM, Dresselhaus MS, Chen G, Ren ZF (2008) Science 320:5876
11. Saleemi M, Toprak MS, Li S, Johnsson M, Muhammed M (2012) J Mater Chem 22:725
12. Scheele M, Oeschler N, Meier K, Kornowski A, Klinke C, Weller H (2009) Adv Funct Mater 19:3476
13. Nikitin EN, Bazanov VG, Tarasov VI (1961) Sov Phys Solid State 3:2648
14. Harman TC, Taylor PJ, Spears DL, Walsh MP (2000) J Electron Mater 29:L1
15. Thermoelectric Materials of the Future, http://www.marlow.com/resources/futureconcepts/materials.html Accessed June 9 2010
16. Bose S, Acharya HN, Banerjee HD (1993) J Mater Sci 28:5461. doi:10.1007/BF00367816
17. Wang L, Qin XY (2003) Scripta Mater 49:243
18. Rowe DM (2006) Thermoelectrics handbook macro to nano. CRC Press LLC, Boca Raton
19. Zaitsev V, Ktitorov S, Fedorov M (2009) CRC handbook of thermoelectrics. CRC Press LLC, Boca Raton
20. Schilz J, Riffel M, Pixius K, Meyer HJ (1999) Powder Technol 105:149
21. Wei X, Ying QX, Guang KM, Li C (2006) Trans Nonferrous Met Soc 16:987
22. Ioannou M, Hatzikraniotis E, Lioutas C, Hassapis T, Altantzis T (2012) Powder Technol 217:523
23. Lutterotti L, Matthies S, Wenk H-R, Schultz AS, Richardson JW (1997) J Appl Phys 81:594
24. Nanko M, Abe H, Takeda M, Homma T, Abe H, Kondo A, Naito M (2011) Mater Sci Eng 21:012006. doi:10.1088/1757-899X/21/1/012006
25. Fiameni S, Boldrini S, Battiston S, Famengo A (2012) J Solid State Chem 193:142
26. Jung JY, Kim IH (2010) Elec Mater Lett 6(4):187
27. Akasaka M, Iida T, Nemoto T, Soga J, Sato J, Makino K, Fukano M, Takanashi Y (2007) J Crys Growth 304:196
28. Martin JJ (1972) J Phys Chem Solids 33:1139
29. Bux SK, Yeung MT, Toberer ES, Snyder GJ, Kanerb RB, Fleuriala JP (2011) J Mater Chem 21:12259
30. Paul B, Banerji P (2009) Nanosci Nanotechnol Lett 1:208
31. Cederkrantz D, Farahi N, Borup KA, Iversen BB, Nygren M (2012) J Appl Phys 111:023701